Electronic Supplementary Information

Experimental section

Materials: Juncus effusus fibers were purchased from Jiangxi *Juncus effusus* Co., Ltd., Jiangxi, China. Tetrabutyl titanate ($C_{16}H_{36}O_4Ti$, TBT), acetic acid (CH_3COOH), sodium sulfate anhydrous (Na_2SO_4), hydrochloric acid (HCl), ammonium chloride (NH_4Cl), sodium hypochlorite (NaClO), sodium hydroxide (NaOH), sodium salicylate ($C_7H_5O_3Na$), sodium nitroferricyanide (III) dihydrate ($Na_2Fe(CN)_5NO{\cdot}2H_2O$), para-(dimethylamino) benzaldehyde ($C_9H_{11}NO$), and Nafion solution (5 wt%) were purchased from Aladdin Co., Ltd. (Shanghai, China). Absolute ethanol (C_2H_5OH), and hydrazine hydrate ($N_2H_4{\cdot}H_2O$) were purchased from Beijing Chemical Corporation. Carbon paper was purchased from Taiwan CeTech Company. The deionized water used throughout all experiments was purified by a Millipore system. All chemical reagents were used as purchased without further purification.

Preparation of TiO_2/JE-CMTs hybrid: Firstly, the juncus effusus (designated as JE) fibers were washed with ethanol and deionized water, and then dried at 60 °C. Subsequently, 20 mL of ethanol, 2 mL of acetic acid, and 3 g of $C_{16}H_{36}O_4Ti$ were mixed to form a homogeneous solution, followed by 0.15 g of pretreated JE was directly immersed into the mixture and dried at 60 °C overnight. After the evaporation of ethanol, the JE was treated at 800 °C in an argon atmosphere for 2 h at a heating rate of 2 °C min^{-1}. After cooling to room temperature naturally, the resulting product was immersed in a 2 M HCl solution for 24 h, and washed repeatedly with deionized

water until pH = 7 to remove metal residues. Finally, it was dried in a vacuum at 60 °C and designated as TiO_2/JE-CMTs. For comparison, pure TiO_2 power was prepared via a similar procedure without the presence of JE. In addition, the control sample JE-CMTs was directly obtained through the same calcination conditions.

Preparation of TiO_2/JE-CMTs/CP: Typically, 10 mg of catalyst and 40 μL of the 5 wt% Nafion solution were dispersed in 720 μL of absolute ethanol and 240 μL of deionized water by sonicating for 1 h to form a uniform ink. Then 10 μL of the above dispersion was loaded onto a 1 cm^2 carbon paper (CP) and dried under ambient conditions.

Characterizations: X-ray powder diffraction (XRD) patterns were collected on a Shimadzu XRD-6100 diffractometer (Shimadzu, Japan) with a Cu Kα X-ray source. Scanning electron microscopy (SEM) images and corresponding energy-dispersive X-ray (EDX) elemental mapping images were collected on a GeminiSEM 300 scanning electron microscope (ZEISS, Germany) at an accelerating voltage of 5 kV. Transmission electron microscopy (TEM) images were conducted on a Zeiss Libra 200FE transmission electron microscope at an acceleration voltage of 200 kV. Raman spectra are obtained by a LabRAM HR Evolution Raman spectroscopy. X-ray photoelectron spectroscopy (XPS) measurements were carried out on an ESCALAB 250Xi spectrometer equipped with monochromatized Al Kα radiation. Nitrogen adsorption-desorption isotherms of TiO_2/JE-CMTs were performed on a Micromeritics Instrument Corporation ASAP 2460 surface area analyzer at 77 K. The

specific surface area was measured by Brunauer-Emmett-Teller (BET) analysis, and the pore size distribution was obtained by the Barrett-Joyner-Halenda (BJH) method. Thermogravimetric analysis (TGA) was performed on a Perkin-Elmer Model Pyris1 TGA apparatus from 25 to 800 °C at a heating rate of 10 °C min^{-1} in air. UV-vis spectroscopy measurements were performed on a Shimadzu UV-1800 UV-vis spectrophotometer. The ion chromatography (IC) data were obtained by using a ThermoFisher ICS 5000 plus IC.

Electrochemical measurements: The electrochemical measurements were carried out in a gastight H-type cell separated by a Nafion 211 membrane using a three-electrode configuration. Before NRR tests, the Nafion membrane was pretreated by heating in the 3% H_2O_2 solution and 0.5 M H_2SO_4 at 80 ℃ for 1 h, respectively, and then washing with ultrapure water for another 1 h. We used a CHI760E electrochemical workstation (Shanghai, Chenhua) to conduct electrochemical experiments. In this work, the obtained TiO_2/JE-CMTs/CP, Ag/AgCl/saturated KCl, and graphite rod were used as the working electrode, reference electrode, and counter electrode, respectively. All potentials were converted to the reversible hydrogen electrode (RHE) through calibration (E (*vs* RHE) = E (*vs* Ag/AgCl) + 0.197 V + 0.059 × pH). For N_2 reduction experiments, chronoamperometric tests were conducted in N_2-saturated 0.1 M Na_2SO_4 electrolyte (the Na_2SO_4 electrolyte was purged with N_2 for 30 min before the measurement).

Determination of NH_3: Concentration of produced NH_3 was spectrophotometrically

determined by the indophenol blue method. In detail, 4 mL of the electrolyte from the cathodic chamber was mixed with 50 μL oxidizing solution (ρ_{Cl} = 4 − 4.9 NaClO and 0.75 M NaOH), 500 μL coloring solution (0.4 M $C_7H_6O_3Na$ and 0.32 M NaOH), and 50 μL catalyst solution (1 wt% $Na_2[Fe(CN)_5NO]\cdot 2H_2O$) for 1 h. Absorbance measurements were performed from 500 nm to 800 nm. The concentration-absorbance (at 655 nm) curves were calibrated using standard NH_4^+ solution with a series of known concentrations. The fitting curve (y = 0.617x + 0.0135, R^2 = 0.993) shows a good linear relation of absorbance value with NH_4^+ concentration.

Determination of N_2H_4: The N_2H_4 content in the electrolyte was determined by the method of Watt and Chrisp. The mixture of p-$C_9H_{11}NO$ (5.99 g), HCl (30 mL), and C_2H_5OH (300 mL) was used as a color reagent. Typically, 2 mL of electrolyte was removed from the cathodic chamber and mixed with 2 mL above prepared color reagent. After standing for 10 min at room temperature, the UV-vis absorption spectra were collected at a wavelength of 455 nm. The fitting curve (y = 0.4788x + 0.0471, R^2 = 0.999) shows a good linear relation of absorbance value with N_2H_4 concentration.

Calculations of NH_3 yield and Faradaic efficiency (FE):

NH_3 yield (V_{NH3}) was calculated by the following equation:

$$V_{NH3} = c(NH_3) \times V / (t \times m_{cat.}) \quad (1)$$

The amount of NH_3 was calculated as follows:

$$m_{NH3} = c(NH_3) \times V \quad (2)$$

FE was calculated according to the following equation:

$$FE = 3F \times c(NH_3) \times V / (17 \times Q) \times 100\% \quad (3)$$

Where $c(NH_3)$ is the measured NH_3 concentration, V is the volume of the cathodic reaction electrolyte (35 mL), t is the reduction time (2 h), $m_{cat.}$ is the mass loading of the catalyst on CP (0.1 mg), F is the Faraday constant (96500 C mol^{-1}), and Q is the total quantity of applied electricity.

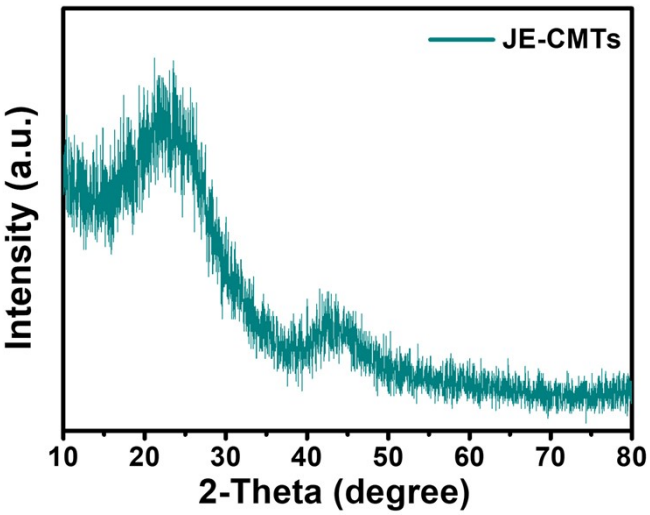

Fig. S1. XRD pattern of JE-CMTs.

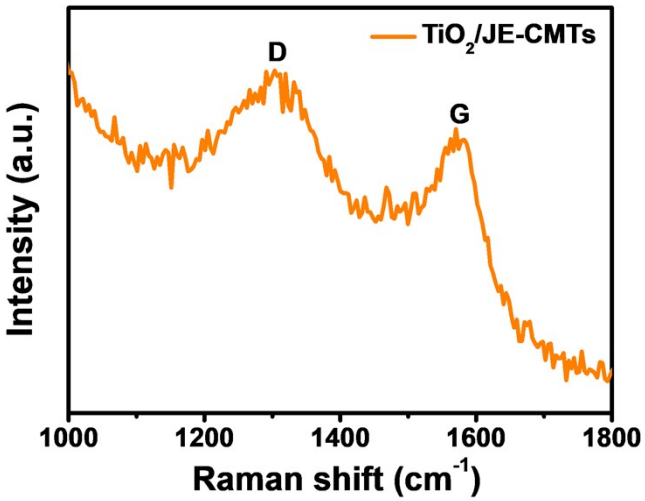

Fig. S2. Raman spectrum of TiO_2/JE-CMTs.

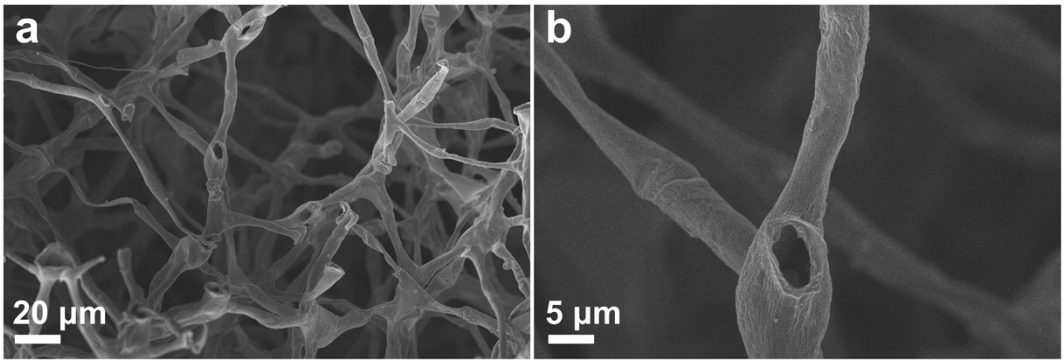

Fig. S3. SEM images of JE-CMTs with different magnifications.

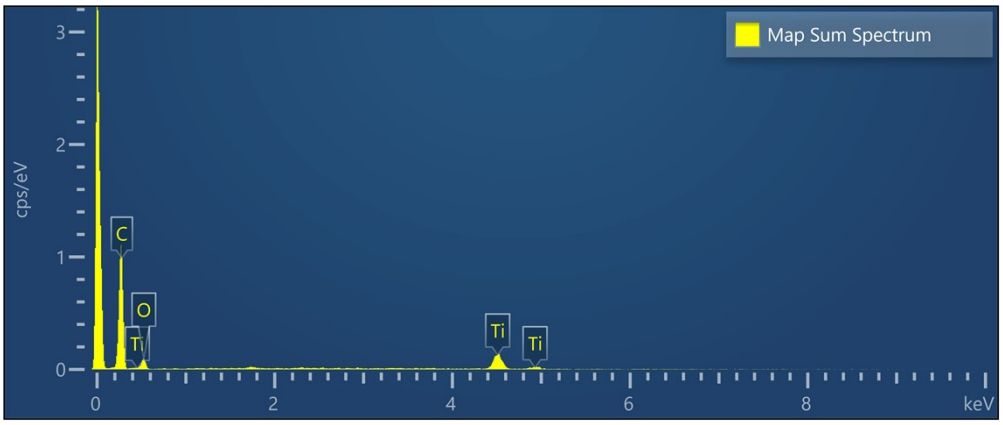

Fig. S4. EDX spectrum of TiO_2/JE-CMTs.

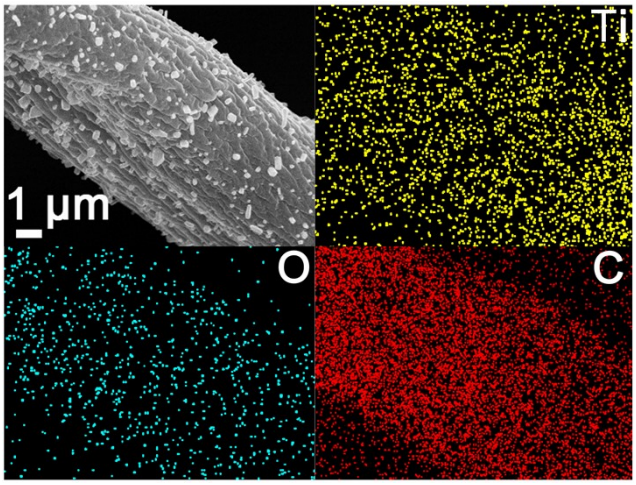

Fig. S5. SEM image and EDX elemental mapping images of Ti, O, and C elements of TiO_2/JE-CMTs.

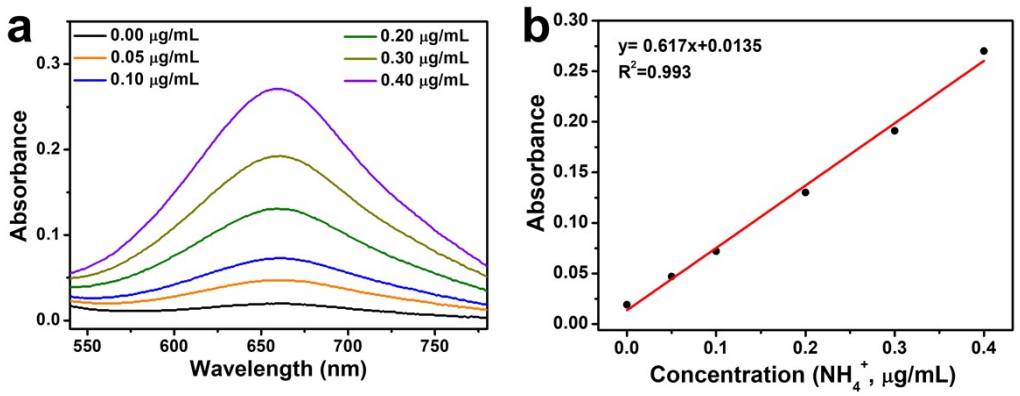

Fig. S6. (a) UV-vis absorption spectra of indophenol assays with NH_4^+ concentrations after incubated for 1 h at room temperature. (b) Calibration curve used for calculation of NH_4^+ concentrations.

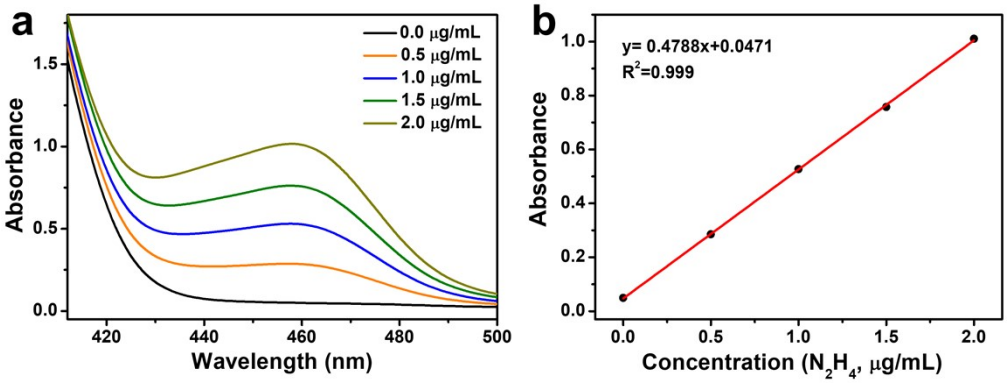

Fig. S7. (a) UV-vis absorption spectra of various N_2H_4 concentrations after incubated for 10 min at room temperature. (b) Calibration curve used for calculation of N_2H_4 concentrations.

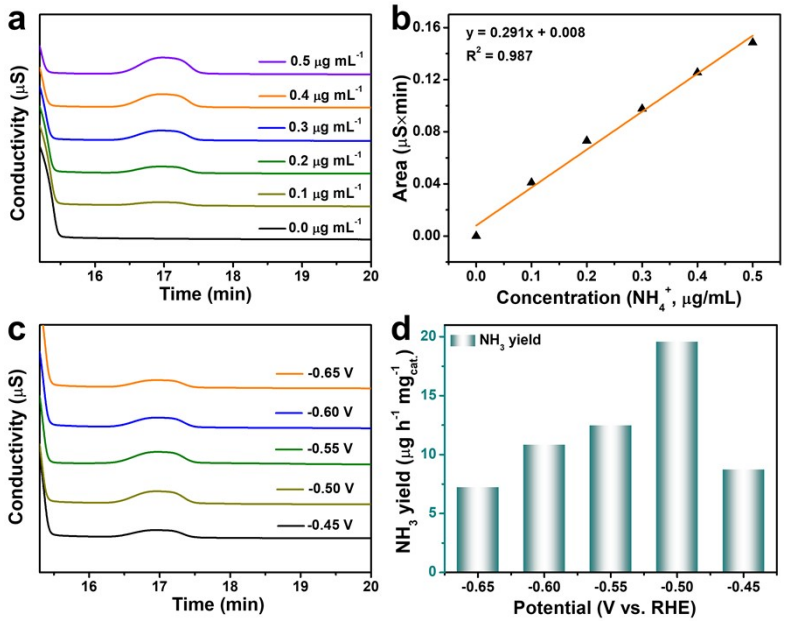

Fig. S8. (a) Ion chromatogram curves of the standard solution with NH_4^+ concentrations in 0.1 M Na_2SO_4. (b) Calibration curve used for estimation of NH_4^+. (c) Ion chromatogram for the electrolytes at a series of potentials after electrolysis for 2 h. (d) NH_3 yields of TiO_2/JE-CMTs/CP at corresponding potentials.

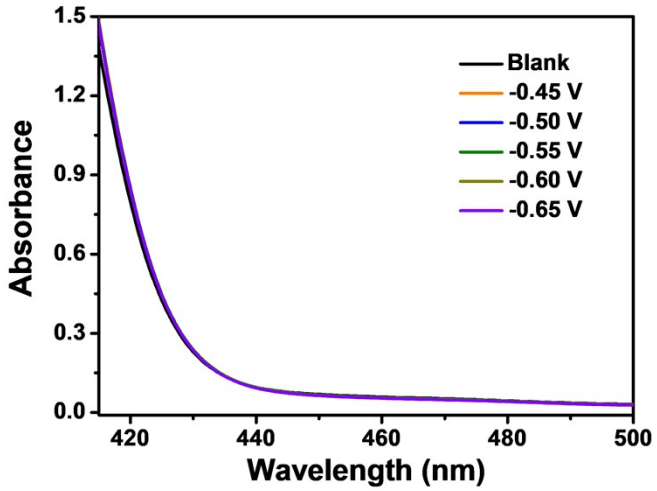

Fig. S9. UV-vis absorption spectra of the electrolytes detected by the method of Watt and Chrisp after 2 h electrolysis in N_2 atmosphere at a series of potentials.

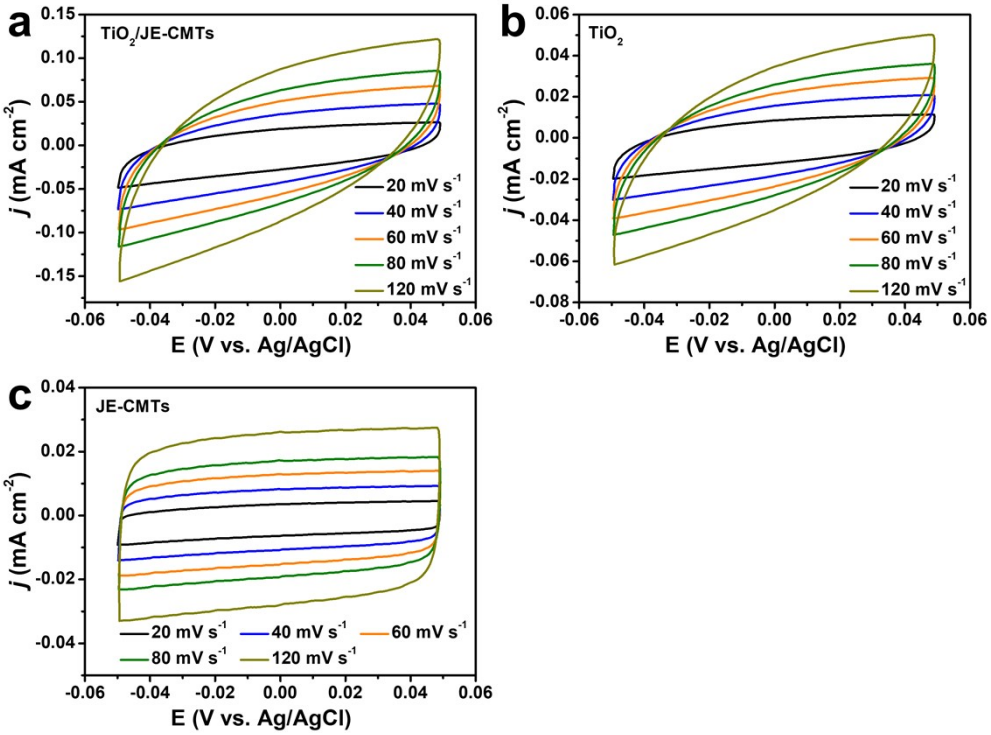

Fig. S10. Cyclic voltammetry curves of (a) TiO_2/JE-CMTs/CP, (b) TiO_2/CP, and (c) JE-CMTs/CP with various scan rates (20−120 mV s^{-1}) in the region of −0.05 to 0.05 V *vs* Ag/AgCl.

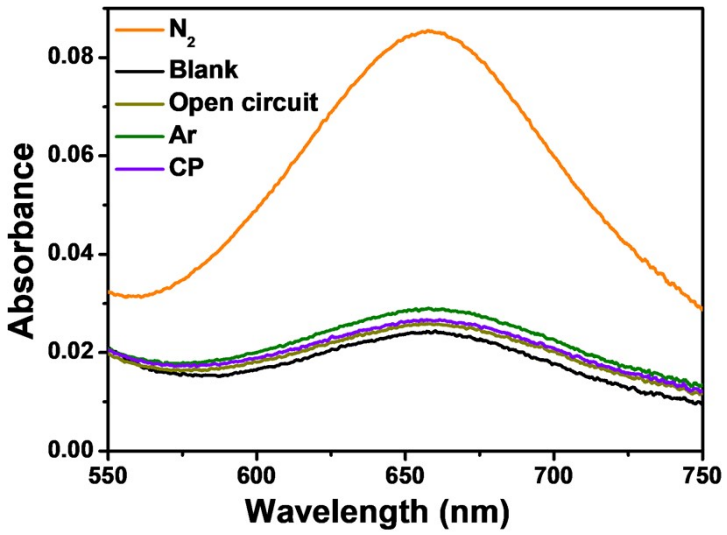

Fig. S11. UV-vis absorption spectra of the electrolytes stained with indophenol indicator for the TiO_2/JE-CMTs/CP electrode after 2 h electrolysis at −0.50 V under different electrochemical conditions.

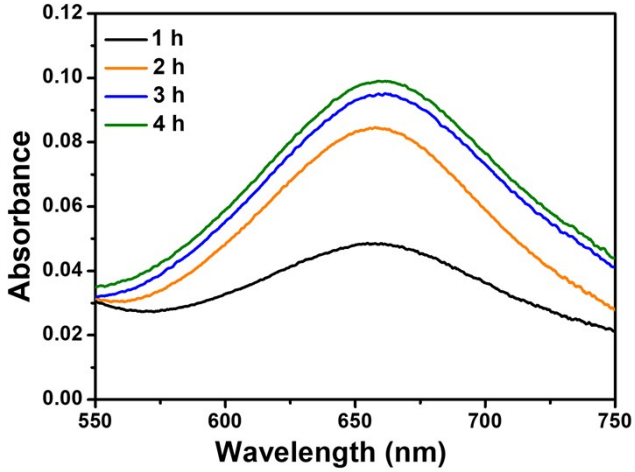

Fig. S12. UV-vis spectra of the electrolytes with different electrolysis time at −0.50 V on the TiO_2/JE-CMTs/CP.

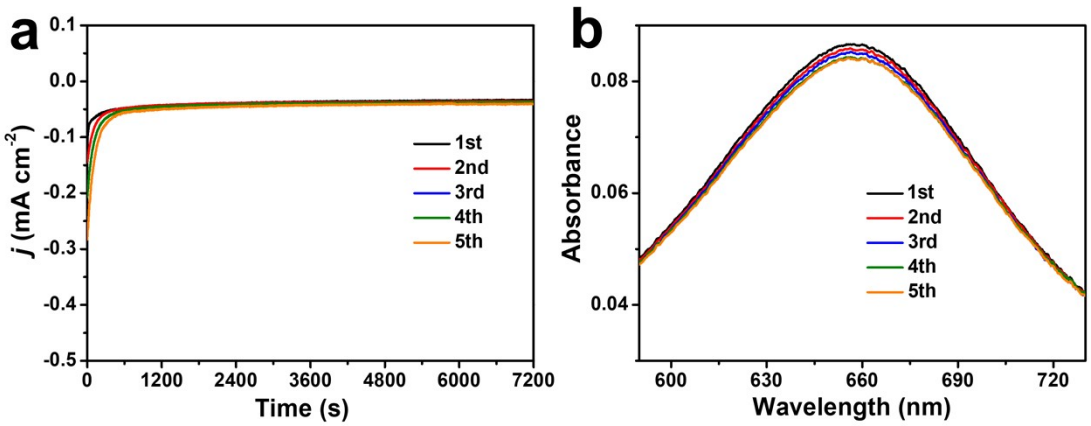

Fig. S13. (a) Chronoamperometry curves of TiO_2/JE-CMTs/CP at −0.50 V in 0.1 M Na_2SO_4 for continuous cycles. (b) UV-vis absorption spectra of the electrolytes stained with indophenol indicator after NRR electrolysis.

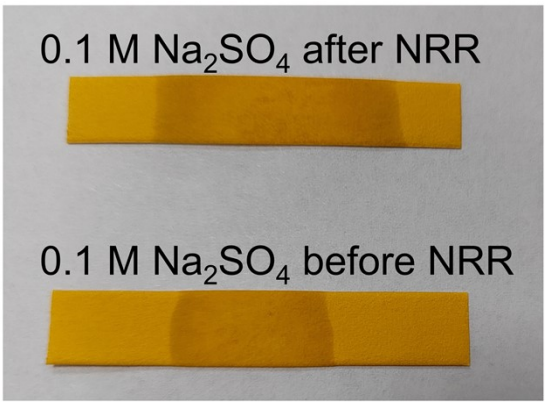

Fig. S14. Photographs of pH test strips in 0.1 M Na_2SO_4 before and after 36-h electrolysis.

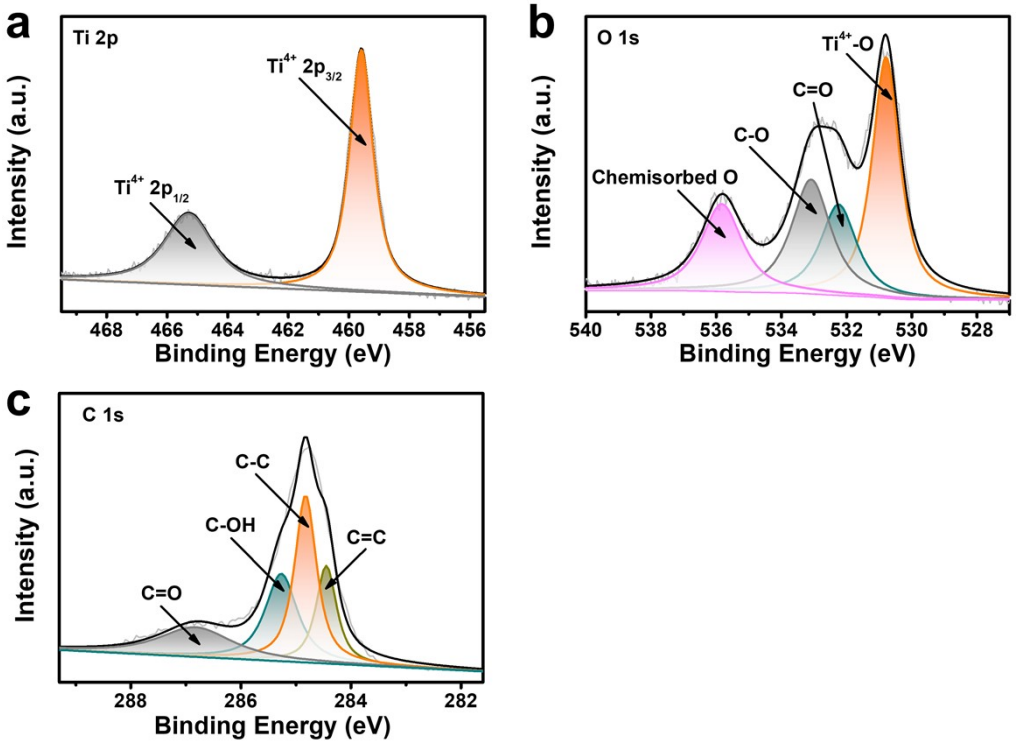

Fig. S15. XPS spectra of TiO_2/JE-CMTs/CP after long-term NRR electrolysis.

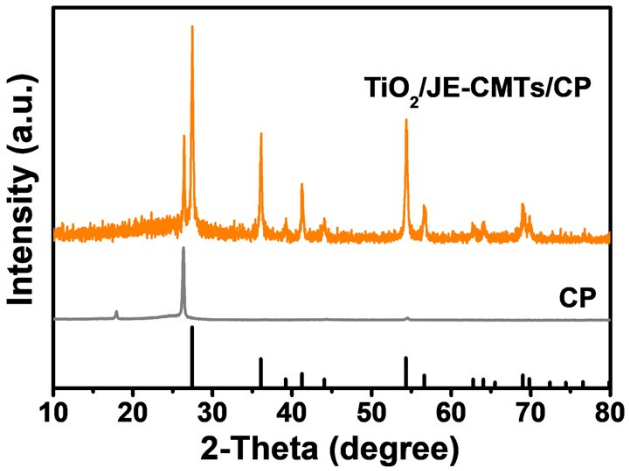

Fig. S16. XRD pattern for TiO_2/JE-CMTs/CP after long-term NRR electrolysis.

Table S1. Comparison of the electrocatalytic NRR performances of TiO_2/JE-CMTs with other reported Ti- and carbon-based NRR catalysts under ambient conditions.

Catalysts	Electrolyte	NH_3 yield	FE (%)	Ref.
TiO_2/JE-CMTs	0.1 M Na_2SO_4	20.03 μg h^{-1} $mg^{-1}_{cat.}$	10.76	This work
C-doped TiO_2	0.1 M Na_2SO_4	16.22 μg h^{-1} $mg^{-1}_{cat.}$	1.84	1
B-doped TiO_2	0.1 M Na_2SO_4	14.4 μg h^{-1} $mg^{-1}_{cat.}$	3.4	2
V-TiO_2	0.5 M $LiClO_4$	17.73 μg h^{-1} $mg^{-1}_{cat.}$	15.3	3
TiO_2/Ti	0.1 M Na_2SO_4	5.6 μg h^{-1} $mg^{-1}_{cat.}$	2.5	4
Ti^{3+}-TiO_{2-x}/TM	0.1 M Na_2SO_4	3.51×10^{-10} mol s^{-1} cm^{-2}	14.62	5
d-TiO_2/TM	0.1 M HCl	1.24×10^{-10} mol s^{-1} cm^{-2}	9.17	6
Y-TiO_2-C	0.1 M HCl	6.3 μg h^{-1} $mg^{-1}_{cat.}$	11.0	7
TiO_2-rGO	0.1 M Na_2SO_4	15.13 μg h^{-1} $mg^{-1}_{cat.}$	3.3	8
C-Ti_xO_y/C	0.1 M Li_2SO_4	14.8 μg h^{-1} $mg^{-1}_{cat.}$	17.8	9
TiC/C NF	0.1 M HCl	14.1 μg h^{-1} $mg^{-1}_{cat.}$	5.8	10
TiB_2 thin film	0.1 M HCl	1.75×10^{-10} mol s^{-1} cm^{-2}	11.37	11
Zr-doped TiO_2	1.0 M KOH	8.9 μg h^{-1} cm^{-2}	17.3	12
Oxygen-doped hollow carbon microtubes	0.1 M HCl	25.12 μg h^{-1} $mg^{-1}_{cat.}$	9.1	13
Reduced graphene oxide	0.5 M $LiClO_4$	17.02 μg h^{-1} $mg^{-1}_{cat.}$	4.83	14
Nitrogen-doped porous carbon	0.005 M H_2SO_4	1.31 mmol h^{-1} $g^{-1}_{cat.}$	9.98	15
S-doped carbon nanosphere	0.1 M Na_2SO_4	19.07 μg h^{-1} $mg^{-1}_{cat.}$	7.47	16
Co/nitrogen-doped carbon	0.1 M KOH	5.1 μg h^{-1} $mg^{-1}_{cat.}$	10.1	17
Fe-N, P co-doped porous carbon	0.1 M NaOH	4.36 μg h^{-1} $mg^{-1}_{cat.}$	5.3	18

References

1 K. Jia, Y. Wang, Q. Pan, B. Zhong, Y. Luo, G. Cui, X. Guo and X. Sun, Enabling the electrocatalytic fixation of N_2 to NH_3 by C-doped TiO_2 nanoparticles under ambient conditions, *Nanoscale Adv.*, 2019, **1**, 961−964.

2 Y. Wang, K. Jia, Q. Pan, Y. Xu, Q. Liu, G. Cui, X. Guo and X. Sun, Boron-doped TiO_2 for efficient electrocatalytic N_2 fixation to NH_3 at ambient conditions, *ACS Sustainable Chem. Eng.*, 2018, **7**, 117−122.

3 T. Wu, W. Kong, Y. Zhang, Z. Xing, J. Zhao, T. Wang, X. Shi, Y. Luo and X. Sun, Greatly enhanced electrocatalytic N_2 reduction on TiO_2 via V doping, *Small Methods*, 2019, **3**, 1900356.

4 R. Zhang, X. Ren, X. Shi, F. Xie, B. Zheng, X. Guo and X. Sun, Enabling effective electrocatalytic N_2 conversion to NH_3 by the TiO_2 nanosheets array under ambient conditions, *ACS Appl. Mater. Interfaces*, 2018, **10**, 28251−28255.

5 B. Li, X. Zhu, J. Wang, R. Xing, Q. Liu, X. Shi, Y. Luo, S. Liu, X. Niu and X. Sun, Ti^{3+} self-doped TiO_{2-x} nanowires for efficient electrocatalytic N_2 reduction to NH_3, *Chem. Commun.*, 2020, **56**, 1074−1077.

6 L. Yang, T. Wu, R. Zhang, H. Zhou, L. Xia, X. Shi, H. Zheng, Y. Zhang and X. Sun, Insights into defective TiO_2 in electrocatalytic N_2 reduction: combining theoretical and experimental studies, *Nanoscale*, 2019, **11**, 1555−1562.

7 L. Yang, C. Choi, S. Hong, Z. Liu, Z. Zhao, M. Yang, H. Shen, A. W. Robertson, H. Zhang and T. W. B. Lo, Single yttrium sites on carbon-coated TiO_2 for efficient electrocatalytic N_2 reduction, *Chem. Commun.*, 2020, **56**, 10910−10913.

8 X. Zhang, Q. Liu, X. Shi, A. M. Asiri, Y. Luo, X. Sun and T. Li, TiO_2 nanoparticles–reduced graphene oxide hybrid: an efficient and durable electrocatalyst toward artificial N_2 fixation to NH_3 under ambient conditions, *J. Mater. Chem. A*, 2018, **6**, 17303−17306.

9 Q. Qin, Y. Zhao, M. Schmallegger, T. Heil, J. Schmidt, R. Walczak, G. Gescheidt-Demner, H. Jiao and M. Oschatz, Enhanced electrocatalytic N_2 reduction via partial anion substitution in titanium oxide–carbon composites, *Angew. Chem., Int. Ed.*, 2019, **58**, 13101−13106.

10 G. Yu, H. Guo, W. Kong, T. Wang, Y. Luo, X. Shi, A. M. Asiri, T. Li and X. Sun, Electrospun TiC/C nanofibers for ambient electrocatalytic N_2 reduction, *J. Mater. Chem. A*, 2019, **7**, 19657−19661.

11 S. Li, Y. Wang, J. Liang, T. Xu, D. Ma, Q. Liu, T. Li, S. Xu, G. Chen, A. M. Asiri, Y. Luo, Q. Wu and X. Sun, TiB_2 thin film enabled efficient NH_3 electrosynthesis at ambient conditions, *Mater. Today Phys.*, 2021, **18**, 100396.

12 N. Cao, Z. Chen, K. Zang, J. Xu, J. Zhong, J. Luo, X. Xu and G. Zheng, Doping strain induced bi-Ti^{3+} pairs for efficient N_2 activation and electrocatalytic fixation, *Nat. Commun.*, 2019, **10**, 2877.

13 T. Wu, P. Li, H. Wang, R. Zhao, Q. Zhou, W. Kong, M. Liu, Y. Zhang, X. Sun and F. F. Gong, Biomass-derived oxygen-doped hollow carbon microtubes for electrocatalytic N_2-to-NH_3 fixation under ambient conditions, *Chem. Commun.*, 2019, **55**, 2684−2687.

14 Y. Song, T. Wang, J. Sun, Z. Wang, Y. Luo, L. Zhang, H. Ye and X. Sun, Enhanced electrochemical N_2 reduction to NH_3 on reduced graphene oxide by tannic acid modification, *ACS Sustainable Chem. Eng.*, 2019, **7**, 14368−14372.

15 C. Zhao, S. Zhang, M. Han, X. Zhang, Y. Liu, W. Li, C. Chen, G. Wang, H. Zhang and H. Zhao, Ambient electrosynthesis of ammonia on a biomass-derived nitrogen-doped porous carbon electrocatalyst: contribution of pyridinic nitrogen, *ACS Energy Lett.*, 2019, **4**, 377−383.

16 L. Xia, X. Wu, Y. Wang, Z. Niu, Q. Liu, T. Li, X. Shi, A. M. Asiri and X. Sun, S-doped carbon nanospheres: an efficient electrocatalyst toward artificial N_2 fixation to NH_3, *Small Methods*, 2019, **3**, 1800251.

17 Y. Gao, Z. Han, S. Hong, T. Wu, X. Li, J. Qiu and Z. Sun, ZIF-67-derived cobalt/nitrogen-doped carbon composites for efficient electrocatalytic N_2 reduction, *ACS Appl. Energy Mater.*, 2019, **2**, 6071−6077.

18 P. Song, H. Wang, X. Cao, N. Liu, Q. Wang and R. Wang, Ambient electrochemical N_2 reduction to NH_3 on nitrogen and phosphorus Co-doped porous carbon with trace iron in alkaline electrolytes, *ChemElectroChem*, 2020, **7**, 212−216.